MedChemComm

RSC Publishing

CONCISE ARTICLE

View Article Online
View Journal

Cite this: DOI: 10.1039/c2md20141k

Design, synthesis and crystal structure determination of dinuclear copper-based potential chemotherapeutic drug entities; *in vitro* DNA binding, cleavage studies and an evaluation of genotoxicity by micronucleus test and comet assay†

Farukh Arjmand,*[a] Mohd Muddassir,[a] Yusra Zaidi[b] and Debashis Ray[c]

Copper-based potential chemotherapeutic complexes **1** and **2** were designed, synthesized and evaluated for *in vitro* DNA binding, cleaving capability and *in vivo* genotoxicity. The structural elucidation of complexes was done using elemental and spectroscopic data while the (*R*)-enantiomer of Cu(II) complex **1** was studied by single crystal diffraction. *In vitro* DNA binding profiling of both (*R*)- and (*S*)-enantiomers of complexes **1** and **2** was carried out to evaluate their enantioselectivity, exhibiting a remarkable degree of enantioselectivity in their interaction with DNA, with the (*R*)-enantiomer exhibiting greater DNA binding propensity. Interaction between complexes and pBR322 DNA was evaluated by agarose gel electrophoresis assay; both the (*R*)-enantiomeric complexes exhibit effective DNA cleavage and proceed *via* an oxidative pathway. Furthermore, the *in vivo* genotoxicity of the (*R*)-enantiomer of complex **1** was evaluated by micronucleus testing on bone marrow cells and comet assay in peripheral blood lymphocytes. These results support our contention that the (*R*)-enantiomer of complex **1** is a suitable chemotherapeutic drug candidate showing reduced toxic effects on normal cells as compared to cisplatin and an antioxidant (EVOO).

Received 30th May 2012
Accepted 27th November 2012

DOI: 10.1039/c2md20141k

www.rsc.org/medchemcomm

Introduction

Cisplatin, *cis*-diamminedichloroplatinum(II) or CDDP, is the most striking example of an anticancer drug widely used clinically in modern medicinal chemistry.[1] CDDP is highly effective in treating a variety of solid tumors, including testicular (cancer which was incurable prior to cisplatin therapy) for which the overall cure rate exceeds 90%.[2]

Cisplatin exerts its mode of action as a consequence of covalent bonding to the natural structure of double helix DNA. More than 90% of CDDP adducts are DNA cross-links. If enough of these adducts are produced without repair, the cell undergoes apoptotic death. This process is not selective, cisplatin interacts with non-cancerous (healthy or normal) cells and biomolecules producing secondary effects that limit the dose that can be administered.[3] In addition, cisplatin is also associated with systemic toxicity and inherent or intrinsic resistance. Genotoxicity of CDDP and other anticancer drugs which exhibit a mechanism of action similar to cisplatin is a serious problem due to the possibility of inducing secondary tumors or 'metastasis'.[4] To address this issue, optimization of the chemical entities to exert specific chemotherapeutic action *in vitro* and *in vivo* is being carried out by many researchers worldwide.[5–7]

Chiral drugs are at the forefront of pharmaceutical drug research as introduction of chirality not only enforces stereoselective specific drug interaction but also promotes the formation of active compounds with therapeutic benefits as most of the biotargets *viz.*, DNA (the primary intracellular target) are chiral in nature. Enantioselective interaction plays a pivotal role in drug DNA adducts formation and provides clues on metal complex coordination to DNA helix (binding mode). Furthermore, the use of stereochemistry can give clear insight into the mechanism of action allowing the discrimination between unspecific interaction which is common to both enantiomers and specific contacts that give rise to enantioselectivity. In view of this, we have designed copper-based complexes **1** and **2** which are chiral in nature derived from reduced Schiff base ligands of salicylaldehyde/benzaldehyde and (*R*)- and (*S*)-2-amino-1-propanol. These complexes bear novelty because of (i) reduced Schiff base skeletons which are more flexible and stable, (ii) chiral stereogenic carbon centres,

[a]*Department of Chemistry, Aligarh Muslim University, Aligarh-202002, India. E-mail: farukh_arjmand@yahoo.co.in; Tel: +91 5712703893*

[b]*Department of Zoology, Aligarh Muslim University, Aligarh-202002, India*

[c]*Department of Chemistry, Indian Institute of Technology, Kharagpur, 721302, India*

† Electronic supplementary information (ESI) available. CCDC 765605. For ESI and crystallographic data in CIF or other electronic format see DOI: 10.1039/c2md20141k

(iii) bio-essential copper centres which show high nucleobase affinity capable of efficient DNA cleavage, (iv) dinuclear redox active copper centres (redox activity of metal complexes is correlated with their anti-proliferative properties) and (v) exceptional DNA cleaving capability. We have validated DNA binding potential and cleavage ability of (*R*)- and (*S*)-enantiomers of **1** and **2** to evaluate their enantiopreferential selectivity. Apart from the modulation of the drug design, the possible role of dietary antioxidants (EVOO) in combination with anticancer agents can be promising to minimize or avoid primary genetic damage and therefore the effects of olive oil in the presence of the complex **1b** as a potential chemotherapeutic drug candidate and also with CDDP have been evaluated. Considering the role of DNA damage in some diseases, the evaluation of the genotoxicity and protective effects of small molecules or therapeutic compounds has become very important. The micronucleus (MN) assay on peripheral blood or bone marrow cells is considered the primary assay for assessing *in vivo* genotoxic potential.[8] The alkaline comet assay complements the MN test.[9] We have analyzed the *in vivo* genotoxicity of these complexes by micronucleus testing on bone marrow cells and comet assay in peripheral blood lymphocytes. This is the first report to the best of our knowledge on the protective effect of EVOO against damage induced by CDDP and complex **1b**. Overall, these chiral complexes exhibit potential to act as promising specific anti-tumor drugs with reduced toxicity.

Results and discussion

The synthesis involves *in situ* reduction (by $NaBH_4$) of a Schiff base of salicylaldehyde/benzaldehyde and (*R*)- and (*S*)-2-amino-1-propanol to yield the ligand **L1** and **L2** (**a** and **b**), respectively. Subsequently, complexes **1** and **2** were synthesized and thoroughly characterized (Scheme 1). Complexes **1** and **2** are stable toward air and moisture and soluble in H_2O and other common solvents. Molar conductance values of complexes reveal their non-electrolytic nature. *In vitro* DNA binding and cleavage of both enantiomeric complexes was carried out to evaluate their enantioselective preference.

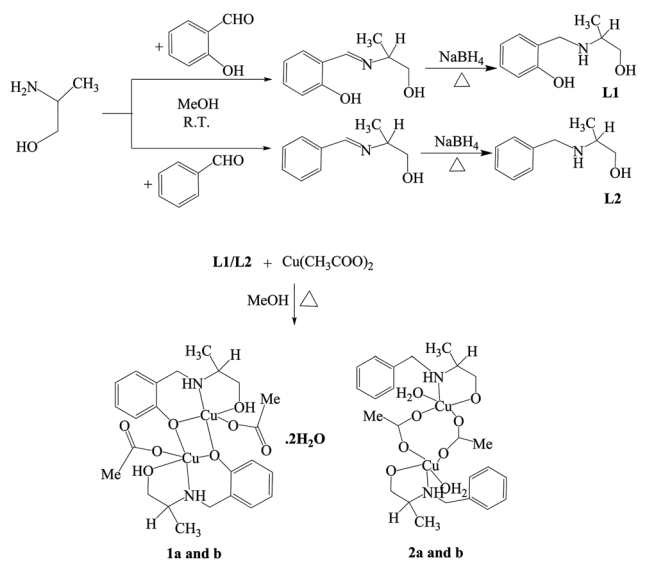

Scheme 1 Synthetic scheme of ligands **L1**, **L2** and complexes **1** and **2**.

Synthesis and characterization

IR spectroscopy is one of the useful techniques used to assign the carboxylate coordination modes, and the following trend is generally accepted as a guideline to differentiate various carboxylate coordination modes, $\Delta\nu$ chelating < $\Delta\nu$ bridging < $\Delta\nu$ ionic < $\Delta\nu$ monodentate.[10] Complex **1** revealed intense bands at 1632 cm^{-1} for ν_{asym} (OCO) and at 1391 cm^{-1} for ν_{sym} (OCO), respectively. The $\Delta\nu = 241$ cm^{-1} value of complex **1** was higher than that reported for sodium acetate ($\Delta\nu = 164$ cm^{-1}), and thus indicates a monodentate acetate coordination mode.[11] Complex **2** revealed one band at 1636 cm^{-1} assignable to ν_{asym} (OCO) and one band at 1479 cm^{-1} assignable to ν_{sym} (OCO) and the calculated $\Delta\nu = 157$ cm^{-1} corresponded to *syn–syn* bidentate bridging.[12] The characteristic HC=N stretching vibration, which appears at the 1575–1630 cm^{-1} range, was absent in the ligands, clearly supporting the reduction of the imine bond by $NaBH_4$. A broad band around 3450 cm^{-1} suggested the presence of lattice water in **1**.[13] Furthermore, diagnostic IR bands at 3120, 3262 cm^{-1} and 1546, 1543 cm^{-1} due to ν(–NH) and δ(–NH), respectively, for complex **1** and **2** were observed.[14] The presence of bound aqua ligand in the case of **2** has been ascertained by a medium intensity band at 3753 cm^{-1}.

Both complexes **1** and **2** exhibited a broad d–d transition envelope at 661 and 676 nm, respectively consistent with five-coordinate Cu(II) centers having square-pyramidal geometry.[15] The stronger absorption bands at 393 nm of complex **1** were ascribed to a charge transfer transition from the phenolate moieties to the terminal copper ions, however, these bands were absent in complex **2**, because of the presence of the benzaldehyde moiety. The bands around 247 nm and 251 nm were ascribed to π–π^* transition for **1** and **2**, respectively.

EPR spectroscopy has proven to be a valuable tool for the elucidation of the molecular structure of the binuclear copper complexes.[16] The X-band EPR spectra of **1** and **2** were recorded at room and different temperatures in the solid as well as liquid state (ESI, Fig. S1†). The spectra (solid) at room temperature show no hyperfine splitting of **1** and **2** irrespective of temperature variation. The *g* values are given in Table 4.

In solution state (methanol) four hyperfine lines in the spectra of **1** and **2** were observed reflecting the coupling with the Cu(II) nucleus ($I = 3/2$), indicative of the existence of Cu(II)–Cu(II) interactions.[17] No effect of temperature was observed in the liquid state as it remains the same with the same hyperfine splitting. The trend $g_{\|} > g_{\perp} > 2.02$ reveals that the unpaired electron is present in the $d_{x^2-y^2}$ orbital.[18] For a Cu(II) complex, $g_{\|}$ is a parameter sensitive enough to indicate covalence. For a covalent complex, $g_{\|} < 2.3$ and for an ionic environment, $g_{\|} = 2.3$ or more. In the present complexes $g_{\|} < 2.3$ which indicates an appreciable metal–ligand covalent character.

Description of the crystal structure of 1b

The single crystal X-ray structure determination of complex **1b** was undertaken. All calculations were performed using

SHELXL-97 implemented in the WINGX system of programs. ORTEP views of complex **1b** with atom numbering scheme and thermal ellipsoids are drawn at 30% probability level and are given in Fig. 1 and 2. The crystallographic data are given in Table 1, and the selected bond lengths and angles for the asymmetric unit are given in Tables 2 and 3. The asymmetric part of the unit cell consists of two crystallographically independent and chemically identical units of complex **1b**, units 1(a) and 1(b), respectively and four symmetrically H-bonded water molecules. The asymmetric part represents a $[Cu_2]$ complex bridged by phenolate oxygen (O_{ph}) atoms. Two tridentate deprotonated $[O_{ph}N_{am}O_{1a}H]^-$ ligands bind the Cu^{II} ion in a *facial* mode. In the square-pyramidal coordination environment, depending on the axial or equatorial positions, the Cu–O bond distances in the Cu–μ–O_{ph} unit vary within a wide range of 1.936–1.900 Å for **1a** and 1.927–1.981 Å for **1b**, respectively. The combination of two short and two long bonds clearly indicates the presence of an asymmetric Cu_2O_2 diamond motif.

Further coordination from amine nitrogen (N_{am}), terminal alkoxido oxygen (O_{al}) and acetato oxygen (O_{ac}) atoms completes the distorted N_2O_3 square pyramidal environment around each Cu^{II}. Within the diamond core the Cu1–O_{ph}–Cu2 angles are 102.51°, 102.16° for 1(a) and 101.08°, 103.48° for 1(b). The solid angle around the bridging O_{ph} atoms ranges from 356.2° to 359.84° for a trigonal planar arrangement compared to a trigonal pyramidal structure. The bridging phenolate (O_{ph}) groups provide an intramolecular $Cu^{II}\cdots Cu^{II}$ separation of 3.063 Å and 3.049 Å for 1(a) and 1(b), respectively. The calculation of the least-squares planes defined by the atoms of the square-planar coordination plane including the central metal atom shows the copper ions to be displaced from the basal planes toward the alkoxido oxygen atom by 0.764 (Cu1) and 0.253 Å (Cu2) of 1(a) and 0.208 (Cu3) and 0.317 Å (Cu4) of 1(b), respectively. The symmetry of the coordination spheres around the two Cu^{II} ions measured by the Addison parameter (τ)[19] is best described by distorted square pyramids with τ values for Cu1, Cu2, Cu3 and Cu4 as 0.22, 0.33, 0.17 and 0.10,respectively. Thus, the Cu2 center is more distorted with a shorter Cu–O_{ph} distance of 1.936 Å for greater bonding interaction with the bridging phenolate oxygen atom. On the basis of the coordination sphere symmetry, it was proposed that at the square pyramid coordination limit (near $\tau = 0$) the magnetic orbitals are mainly $d_{x^2-y^2}$ and weak ferromagnetic interactions should result.[20] The Cu–N_{am} distances (av. 2.007 Å for 1(a) and av. 2.005 Å for 1(b)) are in the normal range. The av. *apical* Cu–O_{al}H distances (2.236 Å in 1(a) and 2.298 Å in 1(b)) are longer than the av. Cu–O_{ac} distances (2.006 Å in 1(a) and 1.964 Å in 1(b)). The terminal monodentate acetate groups having pendant carboxyl oxygen atoms show an extensive H-bonding network with four

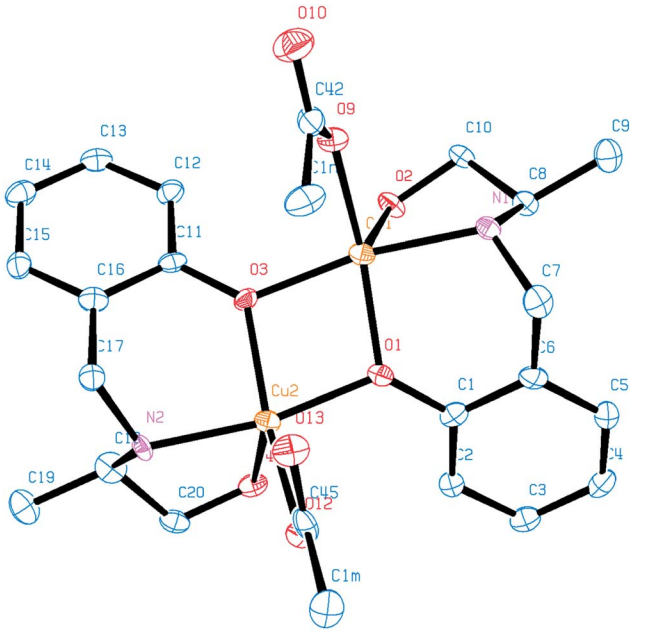

Fig. 2 One unit of labeled ORTEP view of **1b** with atom numbering scheme. H atoms and water molecules are omitted for clarity.

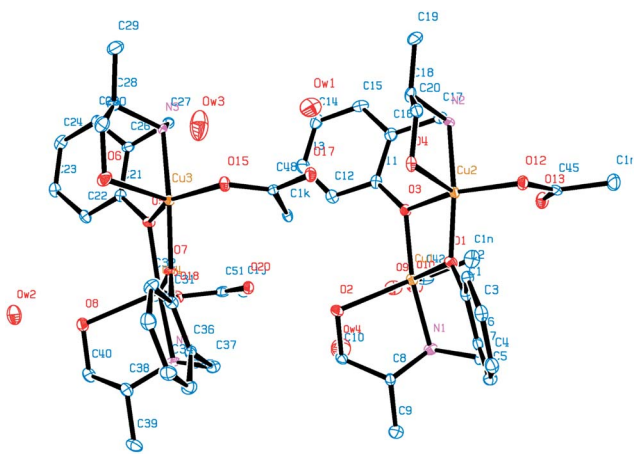

Fig. 1 ORTEP view of **1b** with atom numbering scheme. H atoms are omitted for clarity.

Table 1 Crystallographic data for complex **1b**[a]

CCDC no.	CCDC 765605
Color	Blue
Molecular formula	$C_{24}H_{34}N_2O_{10}Cu_2$
Molecular weight	637.63
Crystal system	$P\bar{1}$
Space group	Orthorhombic
a (Å)	12.104(3)
b (Å)	16.437(4)
c (Å)	27.634(7)
U (Å^3)	5498(2)
D_c (g cm^{-3})	1.531
Z	8
F(000)	2608
Crystal size (mm)	0.06 × 0.09 × 0.19
μ (mm^{-1})	1.603
θ range (°)	2.09–28.43
R_1, wR_2 [$I > 2\sigma(I)$]	0.0650, 0.0995
Goodness-of-fit on F^2	1.064
Final difference map max., min. (e Å^{-3})	1.210, −0.838

[a] $R_1 = \sum(||F_o| - |F_c||)/\sum|F_o|$; w$R_2 = [\sum w(|F_o| - |F_c|)^2/\sum w(F_o)^2]^{1/2}$; $w = 0.75/(\sigma^2(F_o) + 0.0010F_o^2)$.

Table 2 Selected bond lengths [Å] in **1b**

Cu(4)–O(9)	1.956(5)	Cu(1)–O(2)	2.271(5)
Cu(4)–O(11)	1.967(5)	Cu(1)–O(1)	1.990(4)
Cu(4)–N(3)	2.018(5)	Cu(1)–O(3)	1.958(4)
Cu(4)–O(10)	2.282(5)	Cu(2)–O(4)	2.201(5)
Cu(4)–Cu(3)	3.0487(13)	Cu(2)–N(2)	1.999(5)
Cu(3)–O(9)	1.927(4)	Cu(2)–O(3)	1.979(4)
Cu(3)–O(11)	1.981(4)	Cu(2)–O(1)	1.936(4)
Cu(3)–N(4)	1.993(5)	Cu(3)–O(12)	2.315(5)

Table 3 Selected bond angles [°] in **1b**

O(13)–Cu(4)–O(9)	162.7(2)	O(13)–Cu(4)–O(11)	98.0(2)
O(9)–Cu(4)–O(11)	76.87(18)	O(13)–Cu(4)–N(3)	90.3(2)
O(9)–Cu(4)–N(3)	93.1(2)	O(11)–Cu(4)–N(3)	169.0(2)
O(13)–Cu(4)–O(10)	88.9(2)	O(9)–Cu(4)–O(10)	108.36(19)
O(11)–Cu(4)–O(10)	106.84(17)	N(3)–Cu(4)–O(10)	80.3(2)
O(13)–Cu(4)–Cu(3)	132.59(17)	O(9)–Cu(4)–Cu(3)	37.92(13)
O(11)–Cu(4)–Cu(3)	39.62(13)	N(3)–Cu(4)–Cu(3)	129.74(16)
O(10)–Cu(4)–Cu(3)	118.29(12)	O(9)–Cu(3)–O(11)	77.21(19)
O(9)–Cu(3)–N(4)	169.5(2)	O(11)–Cu(3)–N(4)	92.4(2)
O(9)–Cu(3)–O(15)	96.91(19)	O(11)–Cu(3)–O(15)	159.64(19)
N(4)–Cu(3)–O(15)	92.7(2)	O(9)–Cu(3)–O(12)	103.18(18)
O(11)–Cu(3)–O(12)	111.36(17)	N(4)–Cu(3)–O(12)	81.2(2)
O(15)–Cu(3)–O(12)	88.91(18)	O(9)–Cu(3)–Cu(4)	38.60(13)
O(11)–Cu(3)–Cu(4)	39.29(13)	N(4)–Cu(3)–Cu(4)	130.98(17)
O(15)–Cu(3)–Cu(4)	129.55(13)	O(12)–Cu(3)–Cu(4)	117.79(12)
O(1)–Cu(2)–O(3)	77.62(17)	O(1)–Cu(2)–N(2)	171.24(19)
O(3)–Cu(2)–N(2)	93.66(19)	O(1)–Cu(2)–O(8)	97.24(18)
O(3)–Cu(2)–O(8)	151.59(19)	N(2)–Cu(2)–O(8)	90.81(19)
O(1)–Cu(2)–O(4)	101.79(18)	O(3)–Cu(2)–O(4)	117.4(2)
N(2)–Cu(2)–O(4)	81.43(19)	O(8)–Cu(2)–O(4)	91.0(2)
O(3)–Cu(1)–O(1)	76.85(16)	O(3)–Cu(1)–O(5)	95.43(18)
O(1)–Cu(1)–O(5)	154.49(18)	O(3)–Cu(1)–N(1)	168.2(2)
O(1)–Cu(1)–N(1)	91.4(2)	O(5)–Cu(1)–N(1)	95.0(2)
O(3)–Cu(1)–O(2)	105.60(17)	O(1)–Cu(1)–O(2)	112.30(18)
O(5)–Cu(1)–O(2)	93.17(18)	N(1)–Cu(1)–O(2)	79.2(2)
C(11)–O(3)–Cu(1)	131.4(4)	C(11)–O(3)–Cu(2)	122.7(4)
Cu(1)–O(3)–Cu(2)	102.16(19)	C(1)–O(1)–Cu(1)	126.9(4)
Cu(2)–O(1)–Cu(1)	102.51(18)	C(25)–O(9)–Cu(3)	129.0(4)
C(25)–O(9)–Cu(4)	126.9(4)	Cu(3)–O(9)–Cu(4)	103.5(2)
C(35)–O(11)–Cu(4)	131.1(4)	C(35)–O(11)–Cu(3)	127.7(4)
Cu(4)–O(11)–Cu(3)	101.08(19)		

Table 4 EPR parameters of complexes **1b** and **2b**

Complex	$g_{\parallel}$	$g_{\perp}$	g_{iso}	G
1b (solid)	2.0950	2.0379	2.0569	2.5066
1b (liquid)	2.0700	2.0579	2.0610	1.2089
2b (solid)	2.0780	2.0470	2.0570	1.6595
2b (liquid)	2.0700	2.0480	2.0550	1.4583

lattice water molecules. A hexacopper net was generated around three (O1w, O2w and O3w) H-bonded guest water molecules (ESI, Fig. S3†).

Two [Cu_2] complexes trap four water molecules within, which show an intricate H-bonding network with Cu^{II} bound acetate oxygen atoms [O1W···O5 = 2.828 Å; O1W···O7 = 2.778 Å, O1W···O3W = 2.828 Å; O2W···O3W = 2.778 Å, O3W···O8 = 2.828 Å; O12···O7 = 2.778 Å, O2W···O2 = 2.828 Å; O2W···O14 = 2.778 Å, O14···O4W = 2.828 Å; O16···O4 = 2.577 Å]. All these distances are comparable to the O···O distances in ice (about 2.74 Å).[21] The $(H_2O)_3$ trapped supramolecular **1b**···$(H_2O)_3$···**1b** arrangement is shown in Fig. S4.†

DNA binding profile

UV-vis absorption titrations. The absorption spectra of the complexes in the absence and presence of CT DNA at constant concentration of complexes "66.6 × 10^{-6} M" are depicted in Fig. 3 (**1a** and **1b**). With increasing CT DNA (0–33.3 × 10^{-6} M), the absorption bands are affected exhibiting "hyperchromism" 26–39% which reflects higher binding propensity of the complexes for DNA. The labile acetate ion (or water molecule for **2a** and **2b**) of the complexes could be replaced by a nucleophile in DNA, usually a nitrogeneous base such as guanine N7, leading to a strong DNA binding of the complexes.[22] In some cases, binding to the adenine N7 nitrogen has also been observed but to a lesser extent. Complexes **1a** and **1b** undergo blue shift of 5 and 3 nm in π–π*, with a concomitant increase of molar absorptivity, suggesting strong structural and conformational changes involving coordination sphere binding with DNA, while complexes **2a** and **2b** (ESI, Fig. S5†) display a slight increase in molar absorptivity with no appreciable shift. Nevertheless, in both complexes an aromatic moiety is present so the binding of these complexes could also involve partial intercalation of an aromatic ring between the base pairs of DNA.

To further illustrate the enantioselective approach of the complexes, the quantitative comparison of the DNA binding affinities of **1–2** (**a** and **b**) with CT DNA, the intrinsic binding constant K_b values of the complexes were determined by monitoring the change in the absorbance of the π–π* bands with increasing concentration of CT DNA. Furthermore, the K_b values (Table 5) clearly indicate the enantioselective approach of the complexes emphasizing the stronger binding affinity of the (*R*)-enantiomer for DNA as compared to the (*S*)-enantiomer.

Interaction with nucleotides. To obtain concrete information and to determine the coordination of the metal ion to the specific site at the molecular target, interactions with low molecular building blocks of large DNA molecules *viz.*, guanosine-5′-monophosphate, adenosine-5′-monophosphate, cytidine-5′-monophosphate and thymine-5′-monophosphate were carried out with the (*R*)-enantiomer of complexes **1** and **2**. On interaction of **1b** with 5′-GMP, there was a remarkable large red shift (13 nm) in the ligand field band accompanied by a change in the intensity of the bands clearly indicating coordinate covalent binding mode while with other nucleotides *viz.*, 5′-AMP, 5′-CMP and 5′-TMP relatively less blue shift of 6, 6 and 8 nm, respectively, was observed. Interestingly, with CT DNA a red shift of 5 nm was observed (Fig. 4). This reveals that complex **1b** shows preferential interaction toward the guanosine residue by the coordination to the N7 atom of the guanine base of DNA double helix. Our results are in agreement with other interaction studies of Cu(II) complexes with DNA nucleotides using absorption and EPR measurements.[23]

Nonetheless, in the case of complex **2b**, there was relatively small shift on interaction with the nucleotides as well as CT

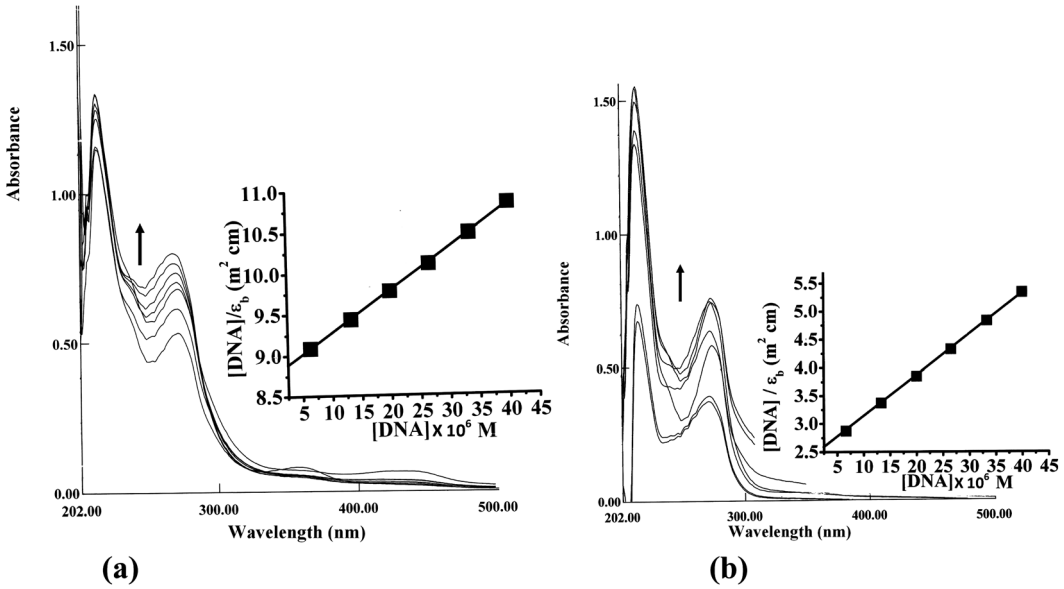

Fig. 3 Absorption spectral traces of **1a** and **1b** (a and b) in Tris–HCl buffer upon addition of CT DNA at 25 °C. Inset: plots of [DNA]/ε_b *vs.* [DNA] for the titration of CT DNA with complexes ■, experimental data points; full lines, linear fitting of the data. [Complex] 6.67 × 10^{-6} M, [DNA] 0–33.3 × 10^{-6} M.

Table 5 The binding constant (K_b) values of complexes with the DNA (mean standard deviation)

Complex	K_b (M^{-1})	% Hyperchromism	Blue Shift
1a	1.11 × 10^4(±0.03)	28	3
1b	5.56 × 10^4(±0.04)	39	5
2a	0.32 × 10^4(±0.04)	26	0
2b	1.30 × 10^4(±0.03)	38	1

DNA (5′-GMP, 5′-CMP, 5′-TMP display a red shift of 1–2 nm, while AMP and CT DNA display a blue shift of 2–3 nm) (Fig. 4). All these parameters are consistent with groove binding in accordance with observations of UV-vis absorption titrations of the complex with CT DNA.

Emission spectral studies. Enantiomeric complexes **1a** and **1b**, **2a** and **2b** emit luminescence in Tris–HCl buffer at room temperature, when excited with light of 246 nm. On addition of increasing concentration of CT DNA to the fixed amount of complexes, there was enhancement of the emission intensity indicative of strong interaction of the complexes with CT DNA as depicted in Fig. 5 (**1a** and **1b**) and ESI, Fig. S6† (**2a** and **2b**). The enhancement of the emission intensity is largely due to the change in the environment of the metal complex and is related to the extent to which the complex gets into a hydrophobic environment inside the DNA.[24]

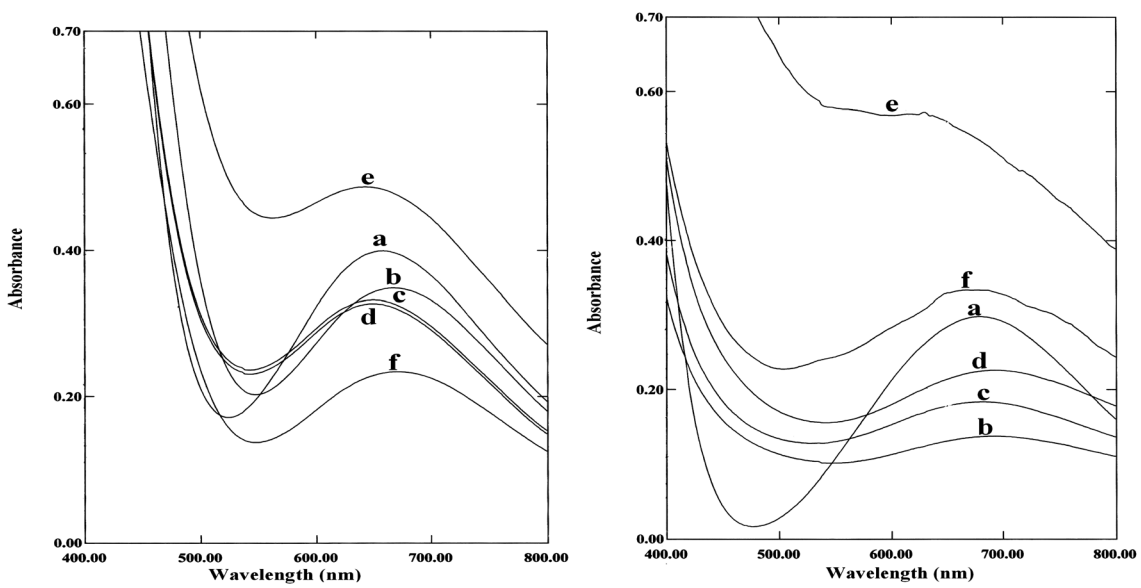

Fig. 4 Absorption spectra of **1b** and **2b** (1 × 10^{-3} M) (a) in Tris–HCl buffer, on interacting with guanosine-5′-monophosphate (b), adenosine-5′-monophosphate (c), cytidine-5′-monophosphate (d), thymine-5′-monophosphate (e) and CT DNA (f) at 10^{-4} M at 25 °C.

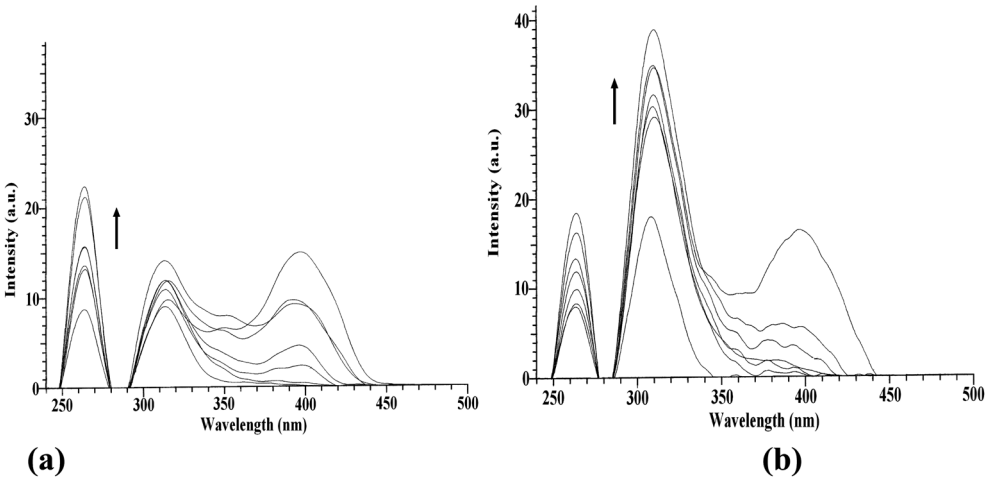

Fig. 5 Emission spectra of **1a** and **1b** (a and b) in Tris–HCl buffer DNA in the presence of DNA at 25 °C. [DNA] 0–33.3 × 10^{-6} M. Arrows show the intensity changes upon increasing concentration of the complexes.

This effect arises because, in the presence of DNA, the metal complex is bound in a relatively non-polar environment compared to water. The binding constant K as quantified by the Scatchard equation[25] for complexes **1a**, **1b**, **2a** and **2b** is found to be 1.14 × 10^4, 5.50 × 10^4, 0.31 × 10^4 and 1.34 × 10^4 M^{-1}, respectively.

EB competition assay. EB emits intense fluorescence in the presence of DNA due to its strong intercalation between the adjacent DNA base pairs. However, the enhanced fluorescence can be quenched evidently when there is a second molecule that can replace the bound EB or break the secondary structure of DNA. The addition of the complexes **1a** and **1b** to DNA pre-treated with EB causes an appreciable reduction in the fluorescence intensity (Fig. 6).

This suggests that complexes **1a** and **1b** compete with EB in binding to DNA.[23] In contrast to complex **1a** and **1b**, emission intensity of complexes **2a** and **2b** (ESI, Fig. S7†) decreases to a smaller extent. But in both complexes (*R*)-enantiomers **1b** and **2b** exhibited a greater decrease as compared to (*S*)-enantiomers.

Circular dichroism. Circular dichroism (CD) is a powerful and sophisticated tool for identifying conformational changes of DNA. The secondary structure of DNA is greatly influenced by interaction of (*R*)- and (*S*)-enantiomers and changes in conformation of DNA from B → Z or B → A. CT DNA in the B conformation shows two conservative CD bands, a positive band at 275 nm due to base stacking and a negative band at 245 nm due to right handed helicity. These bands are sensitive towards binding of any small molecule or drug and hence can be exploited to investigate the binding of small molecules to DNA.[26] Simple groove binding and electrostatic interaction of the complexes with DNA show less or no perturbations on the base stacking and helicity bands while the intercalator enhances the intensities of both the bands. On incubation of present complexes **1a** and **1b**, **2a** and **2b** with CT DNA, the CD spectrum of DNA undergoes changes in both positive and negative bands. Upon the addition of complex **1a**, the CD spectrum of CT DNA displayed an increase in positive and negative ellipticity bands with a small red shift (~2 nm), while

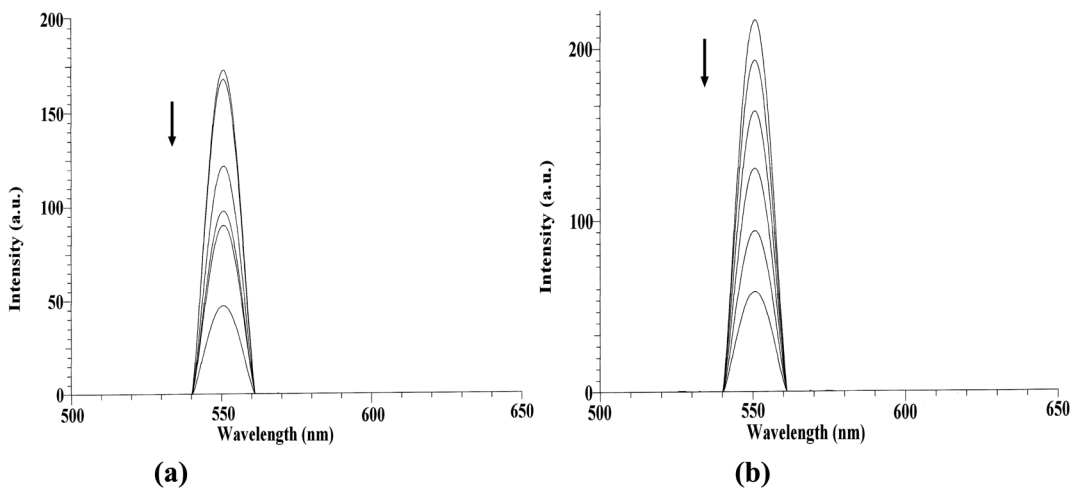

Fig. 6 Fluorescence emission spectra of the EB–CT DNA system in the absence and presence of complexes **1a** and **1b** (a and b) at 25 °C. [Complex], [EB], [DNA] = 10^{-5} M.

in the case of **1b** both positive base stacking and negative helicity bands showed a sharp decrease in comparison to CT DNA alone clearly underlining the enantioselective approach (Fig. 7). Similarly, upon the addition of complex **2a**, the CD spectrum of CT DNA revealed an increase in positive and negative bands without shift in the band position, while in the case of **2b** a reverse effect was observed (as in the case of **1b**) (ESI, Fig. S8†). Therefore, striking differences were observed in CD spectra of complexes on incubating with CT DNA attenuating the effect of enantiomers on biological activity.

DNA cleavage properties

The interactions of pBR322 DNA with (*R*)-enantiomers of complexes **1b** and **2b** were studied in order to determine the DNA cleavage efficiency. When a circular plasmid DNA is subjected to agarose gel electrophoresis, the fastest migration will be observed for the supercoiled form (form I). If one strand is cleaved, the supercoils will relax to produce a slower moving open circular form (form II). If both strands are cleaved, a linear form (form III) will be generated that migrates in between form I and form II .The complexes **1b** and **2b** convert form I into form II, while form III appeared at 0.10 mM for **1b** (lanes 3); however, at the same concentration, other complexes cleave form I DNA into form II but linearized DNA was not observed suggesting that the cleavage may occur randomly over DNA since a significant portion of the plasmid already appears to be transformed into form II without concurrent formation of form III (Fig. S9†).[27]

The most impressive cleavage feature observed for **1b** is that form III DNA appears before the disappearance of form I DNA (lanes 3 and 6) (Fig. S9a†). This phenomenon indicates that this complex is capable of performing direct double-strand scission, while many other copper complexes are only able to cleave single strands successively.[28] The results demonstrate that both complexes **1b** and **2b** are good cleaving agents, however, complex **1b** exhibited higher activity than complex **2b**. Enhancement in hydrophobicity conferred by salicylaldehyde would increase the mobility of the reactive Cu(II) species on DNA, which would also contribute to the higher cleavage activity.[29] The behavior observed for the electrophoretic mobility of these complexes indicates that some conformational changes have occurred. This means that the degree of superhelicity of the DNA molecules has been altered.

In order to identify recognition elements (groove binding) and ROS that are responsible for the DNA cleavage reaction, experiments in the presence of methyl green, DAPI and different common scavengers such as *tert*-butyl alcohol and DMSO (hydroxyl radical scavengers), NaN_3 (singlet oxygen scavenger), D_2O (which is known to increase the lifetime of the O_2) and SOD (superoxide anion radical, $O_2^{\cdot-}$) were carried out, respectively with the *R*-enantiomer. As shown in Fig. 8(a) and (b), complex **1b** inhibits the methyl green (lane 2) as well as DAPI (lane 3) of the DNA digestion, whereas **2b** shows inhibition on methyl green and did not show any effect on DAPI (Fig. 8b). Under these conditions, complex **1b** may bind to both the major as well as the minor groove, whereas complex **2b** binds only to the major groove.

The cleavage activity of **1b** is reduced dramatically by the presence of hydroxyl radical scavengers *tert*-butyl alcohol and DMSO (lanes a4 and a5), indicating that the freely diffusible hydroxyl radical is one of the intermediates involved in the DNA scission process, while complex **2b** has a very slight effect on hydroxyl radical scavengers (lanes b4 and b5).

Singlet oxygen scavenger NaN_3 significantly diminishes the cleavage activity of both the complexes (lanes a6 and b6), suggesting that $^1O_2$ also takes part in the cleavage mechanism. The involvement of $^1O_2$ is also demonstrated by the remarkable enhancement of the cleavage activity in D_2O (lanes a7 and b7), where the lifetime of $^1O_2$ is significantly longer than that in water.[28] Addition of SOD to the reaction mixture shows significant quenching of the cleavage revealing that the superoxide

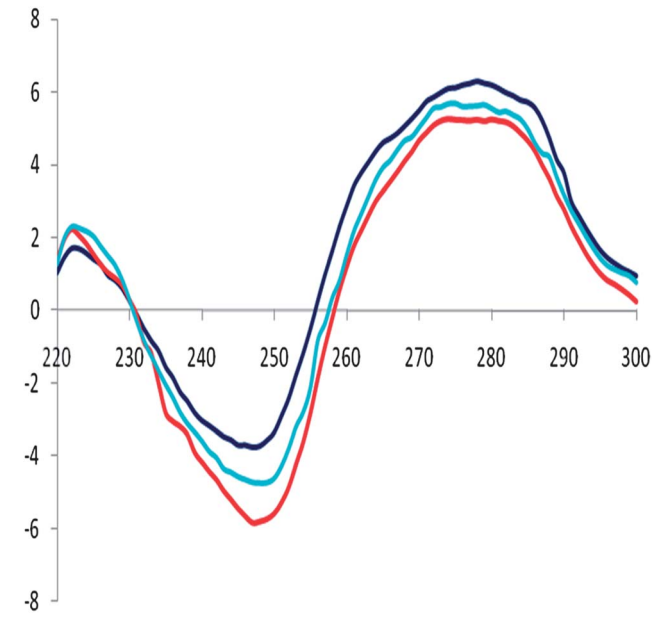

Fig. 7 CD spectra of CT DNA alone and in the presence of **1a** and **1b** in Tris–HCl buffer at 25 °C. [Complex] = 10^{-7} M, [DNA] = 10^{-7} M. The sky blue line represents DNA alone, the dark blue line represents (*S*)-enantiomer interacting with DNA and the red line represents (*R*)-enantiomer interacting with DNA.

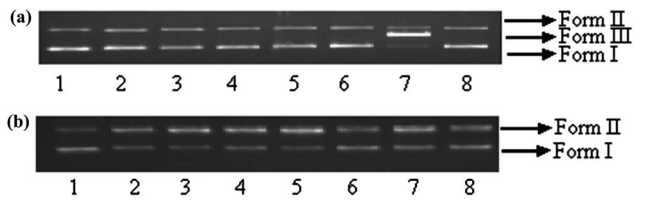

Fig. 8 Agarose gel electrophoresis pattern for the cleavage of pBR322 plasmid DNA (300 ng) by complex **1b** (a) and **2b** (b) (0.20 mmol) in the presence of DNA minor groove binding agent DAPI, major groove binding agent methyl green and different ROS at 25 °C after incubation for 30 minutes. Lane 1, DNA control; lane 2, DNA + metal complex + methyl green (2.5 μL of a 0.01 mg mL^{-1} solution); lane 3, DNA + metal complex + DAPI (8 μM); lane 4, DNA + metal complex + *tert*-butyl alcohol (0.4 mM); lane 5, DNA + metal complex + DMSO (0.4 mM); lane 6, DNA + metal complex + NaN_3 (0.4 mM); lane 7, DNA + metal complex + D_2O (70%); lane 8, DNA + metal complex + superoxide dismutase (15 units), respectively.

anion is also the active species (lanes a8 and b8). In summary, these complexes seem to follow some similar pathways in the cleavage process, in which hydroxyl radicals, singlet oxygen and the superoxide anion are crucial ROS responsible for the cleavage reactions.

Biological studies

***In vivo* genotoxic studies.** We have analyzed the genotoxicity of the complex **1b** *in vivo* rat system by micronucleus (MN) testing on bone marrow cells and comet assay in peripheral blood lymphocytes and compared the results with CDDP. The use of these two tests in conjugation provides additional data indicating whether the DNA damage detected in comet assay resulted in changes that can be detected in the MN test. The data presented here are the first documentation of genotoxic comparison of a new chemotherapeutic metal-based drug candidate with CDDP, furthermore the protective effect of extra virgin olive oil (EVOO) was also studied. CDDP is widely used as a positive control in *in vivo* experiments due to its genotoxic and mutagenic properties.[30–32]

Micronucleus test (MNT). In bone marrow cells, the frequencies of micronucleated polychromatic erythrocytes (MNPCEs) (Fig. 9) significantly increased in CDDP and complex **1b** groups as compared to the control group ($p < 0.05$) but the MNPCEs frequency increased by 1.67 fold in the CDDP group as compared to the **1b** group demonstrating significantly reduced toxicity of complex **1b** (Fig. 10).

Evangelista *et al.* observed that a single dose of EVOO *in vivo* has an anticlastogenic effect against CDDP-induced chromosomal damage in bone marrow cells.[33] The EVOO is remarkably rich in effective phenolic antioxidants that could provide protection by inhibiting oxidative damage.[34,35] Therefore, the effect of EVOO in the presence of CDDP and complex **1b** was also evaluated. EVOO oral post-treatment for 7 consecutive days induced significant decrease of micronucleus frequencies in CDDP as well as **1b** groups as compared to CDDP and **1b** group alone, respectively ($p < 0.05$). This is the first report to the best of our knowledge on the protective effect of EVOO against damage induced by CDDP and complex **1b**. We have also seen the protective effects of EVOO on the formation of MN induced by CDDP and complex **1b** by observing percentage reductions in DNA damage obtained in the micronucleus assay. The results were calculated and are presented in Fig. 11. The reduction in micronucleated cells was more expressive (83.79%) in the group treated with the complex **1b** along with the EVOO and less expressive (33.30%) for the CDDP group orally post treated with EVOO, which validates the effectiveness of antioxidants in reducing the MNPCEs frequency in complex **1b** as compared to CDDP.

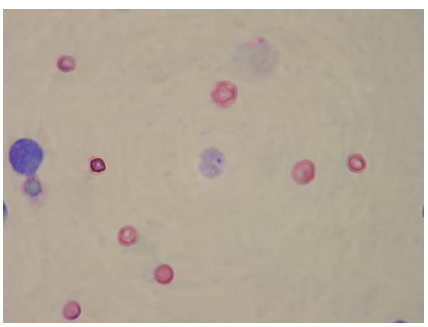

Fig. 9 The micronucleus in polychromatic erythrocytes of bone marrow.

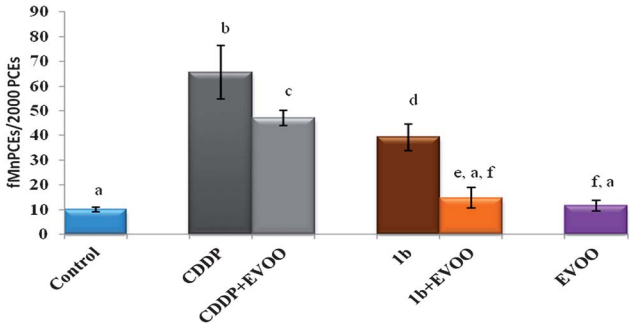

Fig. 10 Frequency of PCEs with micronuclei (fMNPCEs) in a total of 2000 analysed cells per rat in each treatment group to evaluate the mutagenicity of CDDP and **1b** complex and the anti-mutagenicity of the extra virgin olive oil (EVOO). Values are expressed as mean ± SD ($n = 5$). Values that do not share a common superscript letter differ significantly at $p < 0.05$ (one-way ANOVA followed by Tukey's test).

Comet assay. The comet assay is a highly sensitive technique for analysis of DNA damage induced by a drug. CDDP reacts with the nuclear DNA to yield a variety of adducts that include intra- and interstrand DNA–DNA cross-links, as well as DNA–protein crosslinks.[36–39] Under these experimental conditions, analyses of the mean comet tail length (TL) and olive tail moment (OTM) of lymphocytes of CDDP and complex **1b** treated groups were studied as depicted in Fig. S10.† When isolated rat lymphocytes were treated with CDDP and complex **1b**, a greater extent of cellular DNA damage with clear tail lengths was observed in the lymphocytes of CDDP and **1b** treated rats as compared to the control group but the DNA breakage with clear tail length and OTM was significantly higher in lymphocytes of CDDP treated rats as compared to that of the complex **1b** treated group ($p < 0.05$).

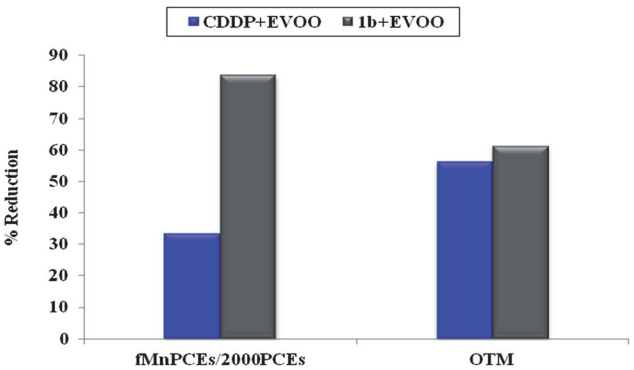

Fig. 11 Percentage of DNA damage reduction promoted by the extra virgin olive oil (EVOO) in the presence of CDDP and **1b** complex, calculated according to the formula of Manoharan and Banerjee and Waters *et al.* The parameters shown are the frequency of micronucleated polychromatic erythrocytes (MNPCEs) and olive tail moment (OTM).

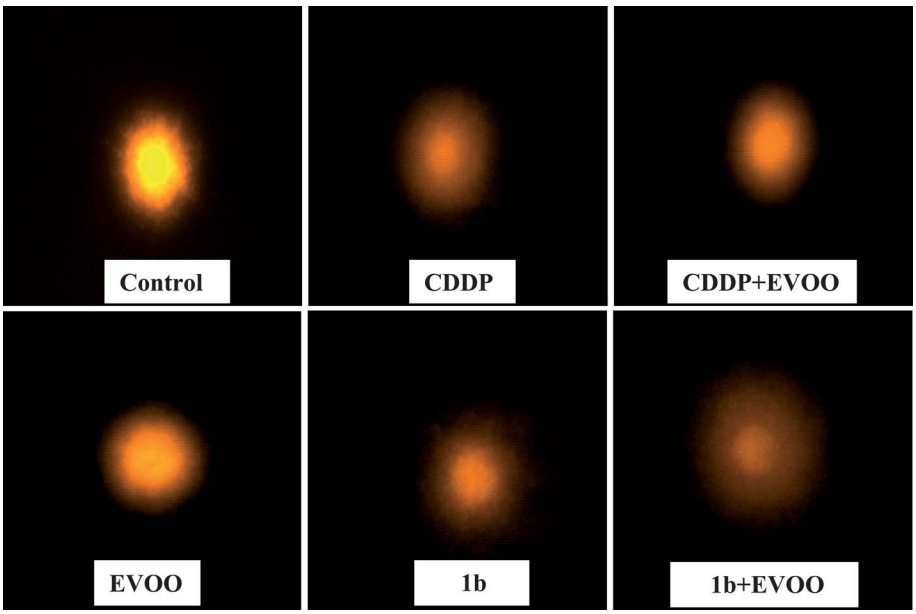

Fig. 12 Representative photographs of comets of peripheral blood lymphocytes treated with CDDP, complex **1b**, and their combination with EVOO.

We also evaluated the antioxidant potential of EVOO in providing protection to lymphocytes against CDDP and complex **1b** induced oxidative injury. The increase in DNA damage was recovered when the rats were orally post treated with EVOO (5 mL per kg body weight) for 7 consecutive days after the CDDP and complex **1b** treatment. Combined treatment of EVOO with CDDP caused significant inhibition of DNA breakage as evidenced by decreased tail length and OTM by 1.69 and 2.03 fold, respectively as compared to the CDDP group alone while the oral administration of EVOO in complex **1b** treated group, the decrease in DNA breakage in terms of tail length and OTM were 1.08 and 1.94 fold, respectively as compared to the **1b** group alone (Fig. 12). The observations of genotoxicity clearly support the contention that copper-based drug candidate complex **1b** exhibits less cellular DNA damage as compared to the cisplatin drug and these results are well corroborated with the observations of MNT.

Experimental section

Materials and measurements

All reagents were of the best commercial grade and were used without further purification. (*S*)-/(*R*)-2-Phenylglycinol, (*S*)-/(*R*)-2-amino-1-propanol (Aldrich), salicylaldehyde (Alfa Aesar), $NaBH_4$, $Cu(CH_3COO)_2 \cdot H_2O$, Tris-(hydroxymethyl)aminomethane–HCl (Tris–HCl) (E. Merck) were used as received. Disodium salt of calf thymus DNA (CT DNA) was purchased from Sigma Chemical Co and was stored at 4 °C. Adenosine-5′-monophosphate disodium salt (5′-AMP), cytidine-5′-monophosphate disodium salt hydrate (5′-CMP), guanosine-5′-monophosphate disodium salt (5′-GMP) and thymine-5′-monophosphate (5′-TMP) were purchased from Fluka and were stored at −20 °C. 6X loading dye (Fermental Life Science), agarose, ascorbic acid, sodium azide (NaN_3), superoxide dismutase (SOD), methyl green, DAPI, mercaptopropionic acid (MPA) (Sigma-Aldrich) and supercoiled plasmid DNA pBR322 (Genei) were utilized as received.

Carbon, hydrogen and nitrogen contents were determined using Carlo Erba Analyzer Model 1108. Molar conductance was measured at room temperature on a Digisun Electronic Conductivity Bridge. Fourier-transform infrared (FTIR) spectra were recorded on an Interspec 2020 FTIR spectrometer in Nujol mull. Electronic spectra were recorded on a UV-1700 PharmaSpec UV-vis spectrophotometer (Shimadzu). Data were reported in λ_{max} (nm). The EPR spectra of the Cu(II) complexes were acquired on a Varian E 112 spectrometer using X-band frequency (9.1 GHz) at liquid nitrogen temperature in the solid state. The ^1H and ^{13}C NMR spectra were obtained on a Bruker DRX-400 spectrometer. Optical rotations of chiral complexes were determined on a Polarimeter Rudolf Autopol III at 25 °C using the sodium D line in DMSO. ESI-MS spectra were recorded on a Micromass Quattro II triple quadrupole mass spectrometer.

Synthesis

Synthesis of (*S*)- and (*R*)-2-((1-hydoxypropan)-2-ylamino) methyl) phenol (L1). 2-Amino-1-propanol (0.75 g, 10 mmol) [(*S*)-2-amino-1-propanol **a**; (*R*)-2-amino-1-propanol **b**] and salicylaldehyde (1.22 g, 10 mmol) were stirred together in methanol (15 mL) for 1 h at room temperature. The resulting yellow colored solution was monitored by TLC for the completion of the reaction and formation of Schiff base. To this solution, $NaBH_4$ (0.46 g, 12 mmol) was added in portions and was refluxed for 2 h, the solution changed color slowly from yellow to colorless. The solvent was removed under vacuum and the residue was dissolved in water (30 mL) and was extracted with $CHCl_3$ (3 × 30 mL). The $CHCl_3$ layers were combined and dried under vacuum. Colorless liquid was formed upon introduction of dry HCl.

(*S*-enantiomer) **a**: $[\alpha]_D^{25} = +72$ (*c* 0.05 in MeOH).

(*R*-enantiomer) **b**: $[\alpha]_D^{25} = -71$ (*c* 0.05 in MeOH).

Both enantiomers exhibited identical IR, Mass, UV-vis and NMR spectra.

Selected IR data on KBr pellet (ν/cm^{-1}): 3217 ν(N–H), 1565 δ(N–H), 2842 ν(CH_2), 1475 ν(C–N), 1390 ν(C–C), 1067 ν(C–$O_{alcohol}$), 1250 ν(C–$O_{phenole}$), 751 ν(Ar); ESI-MS (*m*/*z*) 181 (51%) $[C_{10}H_{15}NO_2]^+$; UV-vis [CH_3OH; λ_{max} nm^{-1}] 308.

δ_H (400 MHz; DMSO-d_6): 1.08 (d, 3H, –CH_3), 2.29 (s, –OH, 1H), 2.85 (m, chiral –CH, 1H), 3.29 (d, –CH_2, 2H), 3.59 (d, –CH_2, 2H), 4.64 (s, –NH), 7.22–7.33 (multiplet, 5H, Ar–H), 7.57 (s, phenol –OH); δ_C (100 MHz; DMSO-d_6): 157.26 (Phenol–OH), 128.53, 128.17, 127.13, 126.99, 126.17 (Ar C), 65.52 (–CH_2OH), 53.78 (chiral C), 51.12 (–CH_2NH).

Synthesis of (*S*)- and (*R*)-2-(benzylamino)propan-1-ol (L2). This was prepared according to a procedure similar to that of **L1** except that 2-amino-1-propanol (0.75 g, 10 mmol) [(*S*)-2-amino-1-propanol **a**; (*R*)-2-amino-1-propanol **b**] was mixed with benzaldehyde (1.09 g, 10 mmol) in methanol (15 mL), followed by *in situ* reduction by $NaBH_4$ and extraction with $CHCl_3$. A colorless liquid was formed upon introduction of dry HCl.

(*S*-enantiomer) **a**: $[\alpha]_D^{25} = +119$ (*c* 0.05 in MeOH).

(*R*-enantiomer) **b**: $[\alpha]_D^{25} = -120$ (*c* 0.05 in MeOH).

Both enantiomers exhibited identical IR, Mass, UV-vis and NMR spectra.

Selected IR data on KBr pellet (ν/cm^{-1}): 3219 ν(N–H), 1557 δ(N–H), 2853 ν(CH_2), 1478 ν(C–N), 1401 ν(C–C), 1043 ν(C–$O_{alcohol}$), 755 ν(Ar); ESI-MS(*m*/*z*) 165 $[C_{10}H_{14}NO+2H]^+$; UV-vis [CH_3OH; λ_{max} nm^{-1}] 313.

δ_H (400 MHz; DMSO-d_6): 1.10 (d, 3H, –CH_3), 2.26 (s, –OH, 1H), 2.69 (m, chiral –CH, 1H), 3.27 (d, –CH_2, 2H), 3.59 (d, –CH_2, 2H), 4.81 (s, –NH), 7.23–7.34 (multiplet, 5H, Ar H); δ_C (100 MHz; DMSO-d_6): 126.95, 126.77, 126.09, 125.83, 125.44 (Ar C), 67.92 (–CH_2OH), 54.98 (chiral C), 54.87 (–CH_2NH).

Synthesis of (*R*)- and (*S*)-[Cu_2^{II}(μ–L1)$_2$(OAc)$_2$]·2H_2O (1). To a methanolic solution (10 mL) of **L1** (**a** and **b**) (0.362 g, 2 mmol) was added a solution of $Cu(CH_3COO)_2 \cdot H_2O$ (0.398 g, 2 mmol) in methanol (10 mL) under refluxing condition for 3 hours. On completion of the reaction, the reaction mixture was kept at room temperature which yielded a blue colored product, washed with hexane and dried *in vacuo*. After filtration, crystals suitable for X-ray diffraction were obtained by slow evaporation of the filtrate after several days.

(*S*-enantiomer) **1a**: yield 49%; m.p. 218–221 °C; Anal. Calc. (%) for $C_{24}H_{38}N_2O_{10}Cu_2$: C, 44.92; H, 5.97; N 4.37. Found: C, 45.03; H, 5.95; N, 4.41; $[\alpha]_D^{25} = +53$ (*c* 0.05 in DMSO); ESI-MS (*m*/*z*): 641 $[C_{24}H_{38}N_2O_{10}Cu_2]^+$.

(*R*-enantiomer) **1b**: yield 46%; m.p. 217–219 °C; Anal. Calc. (%) for $C_{24}H_{38}N_2O_{10}Cu_2$: C, 44.92; H, 5.97; N 4.37. Found: C, 44.86; H, 5.94; N, 4.40; $[\alpha]_D^{25} = -53$ (*c* 0.05 in DMSO); ESI-MS (*m*/*z*): 641 $[C_{24}H_{38}N_2O_{10}Cu_2]^+$.

Both enantiomeric metal complexes exhibited identical IR, UV-vis and EPR spectra.

Selected IR data on KBr pellet (ν/cm^{-1}): 3450 ν(lattice water), 3120 ν(–NH), 2865 ν(–CH_2), 1632 cm^{-1} for ν_{asym}(OCO), 1391 cm^{-1} for ν_{sym}(OCO), 1546 δ(N–H), 1438 ν(C–N), 1354 ν(C–C), 1038 ν(C–$O_{alkoxide}$), 1252 ν(C–$O_{phenolate}$), 752 ν(Ar), 521 ν(Cu–O), 426 ν(Cu–N); UV-vis [CH_3OH; λ_{max} nm^{-1}] 246 (26140), 389 (23890), 661 (90).

Synthesis of (*R*)- and (*S*)-[Cu_2^{II}(μ–OAc)$_2$ (L2·H_2O)$_2$] (2). To a methanolic solution (10 mL) of **L2** (**a** and **b**) (0.330 g, 2 mmol) was added a solution of $Cu(CH_3COO)_2 \cdot H_2O$ (0.398 g, 2 mmol) in methanol (10 mL). The solution was stirred for 4 hours with heating at 80 °C. On completion of the reaction, the reaction mixture was kept at room temperature which yielded a sky blue colored product, washed with hexane and dried *in vacuo*.

(*S*-enantiomer) **2a**: yield 45%; m.p. 224–226 °C; Anal. Calc. (%) for $C_{24}H_{40}N_2O_8Cu_2$: C, 47.28; H, 6.28; N 4.59. Found: C, 47.19; H, 6.25; N, 4.61; $[\alpha]_D^{25} = +68$ (*c* 0.05 in DMSO); ESI-MS (*m*/*z*): 609 $[C_{24}H_{38}N_2O_8Cu_2]^+$.

(*R*-enantiomer) **2b**: yield 44%; m.p. 222–224 °C; Anal. Calc. (%) for $C_{24}H_{40}N_2O_8Cu_2$: C, 47.28; H, 6.28; N 4.59. Found: C, 47.27; H, 6.31; N, 4.62; $[\alpha]_D^{25}$ (DMSO) −67 (*c* 0.05 in DMSO); ESI-MS (*m*/*z*): 610 $[C_{24}H_{38}N_2O_8Cu_2 + H]^+$.

Both enantiomeric metal complexes exhibited identical IR, UV-vis and EPR spectra.

Selected IR data on KBr pellet (ν/cm^{-1}): 3753 ν(coordinated water), 3262 ν(–NH), 2864 ν(–CH_2), 1636 cm^{-1} for ν_{asym}(OCO), 1479 cm^{-1} for ν_{sym}(OCO), 1543 δ(N–H), 1440 ν(C–N), 1397 ν(C–C), 1040 ν(C–$O_{alkoxide}$), 762 ν(Ar), 545 ν(Cu–O), 432 ν(Cu–N).

UV-vis [CH_3OH; λ_{max} nm^{-1}] 251 (25240), 676 (80).

DNA binding experiments

DNA binding experiments which include absorption spectral titrations, luminescence, circular dichoric experiments and DNA cleavage conformed to the standard methods[40–42] and practices previously adopted by our laboratory.[43] While measuring the absorption spectra an equal amount of DNA was added to both the compound solution and the reference solution to eliminate the absorbance of the DNA itself.

Animals and treatment

Adult male Wistar rats, obtained from the animal house of JNMC, Aligarh Muslim University, Aligarh, were used for this study. Rats (150 ± 50 g) were housed in polycarbonate cages with steel wire tops (five animals per group) at standard room temperature (22 ± 2 °C) and humidity (55 ± 10%) with a 12 h light–dark cycle, and received standard food and water *ad libitum*. The day of administration is designated as day 0. The animals were randomly separated and grouped according to age and weight into the following four groups of five rats each. Group I: which received a single dose of DMSO i.p. (intra peritoneal) served as control. Group II: received a single dose of CDDP (5 mg per kg body weight) i.p. Group III: received a single dose of complex **1b** (5 mg per kg body weight) i.p. Group IV: EVOO was administrated orally for 7 consecutive days after a single dose of cisplatin. Group V: administration of EVOO orally for 7 consecutive days after a single dose of complex **1b**. Group VI: administration of EVOO orally for 7 consecutive days alone. At the end of experiments, the rats of each group were sacrificed. By 7 days after drugs and antioxidant administration, blood samples from the rats were collected in tubes containing heparin for comet assay and bone marrow from femur bones

was sampled for micronucleus assay. The experimental protocols for this study were approved by the Local Ethics Committee for Animal of JNMC, AMU, Aligarh.

Micronucleus test

Bone marrow smears and staining were done following the method of Schmid.[44] Briefly, both femurs were removed, and the bone marrow was flushed out into a centrifuge tube with fetal calf serum (FCS). The bone marrow cells were collected by centrifugation at 1000 rpm for 10 min, and the pellet was resuspended in 1 mL FCS for preparation of the slides. A drop of this suspension was smeared on a clean slide, air-dried, fixed in absolute methanol for 5 min and stained the following day with May-Gruenwald and Geimsa stains. Two thousand polychromatic erythrocytes (PCEs) were analyzed for each animal and the number of micronucleated PCEs (MNPCEs) was recorded.

Comet assay

Blood was obtained from different treatment groups *via* cardiac puncture immediately before sacrifice. Samples were heparinized and lymphocytes were isolated from blood by density gradient centrifugation using Histopaque 1077, and the cells were finally suspended in RPMI 1640. The lymphocytes were checked for their viability before the start and after the end of the reaction using the trypan blue exclusion test.[45] The viability of the cells was found to be greater than 93%.

The alkaline version of the comet assay was performed according to the guidelines proposed by Singh, McCoy, Tice, and Scheinder (1998),[46] with a slight modification. Microscope slides pre-coated with 1% normal-melting-temperature agarose were used. Around 1×10^5 cells mixed with 75 μL of 1% LMPA was then layered over the first layer, and left to harden for 5 minutes at 4 °C. Finally a third layer of 0.5% LMPA (75 μL) was layered and left to solidify and covered immediately by a coverslip. This was followed by immersion in ice-cold alkaline lysing solution [2.5 M NaCl, 10 mM Tris, 100 mM EDTA, 1% Triton X-100, final pH 10.0] for at least 1 h at 4 °C. The slides were then incubated for 30 min in ice-cold electrophoresis solution (0.3 M NaOH, 1 mM EDTA, pH > 13), followed by electrophoresis at 0.7 V cm^{-1}: 300 mA current. After electrophoresis, the slides were then neutralized (Tris 0.4 M, pH 7.5) and stained with ethidium bromide (75 microlitre). Fifty cells per mouse (25 cells analysed in each slide) were scored at 100× magnification using an image analysis system (Komet 5.5, Kinetic Imaging, Liverpool, UK) attached to an Olympus (CX 41) fluorescent microscope and a COHU 4910 integrated CC camera.

Statistical analysis

Results are presented as mean values with their standard deviation for experiments. Comparison of mean values between groups was assessed by one-way ANOVA followed by a post-hoc Tukey's test. *P* values of less than 0.05 were considered significant. Data were analyzed using an SPSS statistical software package (SPSS for Windows, version 16).

Conclusion

Enantiomeric dinuclear copper-based potential chemotherapeutic drug candidates **1** and **2** were designed and synthesized to ascertain the structure–activity relationship of these complexes towards DNA. Both enantiomers of **1** and **2** were thoroughly characterized by microanalysis and spectroscopically while the structure of the (*R*)-enantiomer of **1** was elucidated by single crystal X-ray crystallography, which revealed dinuclear Cu(II) complexes exhibiting an unusual acetate bridging structure and diamond core topology. The complexes exhibited square pyramidal geometry around both the Cu(II) centers as ascertained by UV-vis, EPR spectroscopic studies, and by X-ray data in the case of (*R*)-enantiomer **1b**.

Metal complex–DNA interactions were studied by UV-vis, fluorescence, and circular dichroism in both enantiomers of **1** and **2** to validate their potential to act as cancer chemotherapeutic agents as DNA is the primary cellular target of most of the anticancer drugs. Both the complexes bind to DNA by coordinate covalent and groove binding, respectively. Nevertheless, (*R*)-enantiomers bind more strongly in comparison to (*S*)-enantiomers. Therefore, DNA cleavage activity of (*R*)-enantiomers of **1** and **2** was ascertained with pBR322 DNA by agarose gel electrophoretic assay and they followed an oxidative mechanistic pathway in the cleavage process, involving hydroxyl radicals, singlet oxygen and superoxide radicals. The genotoxicity of (*R*)-enantiomer complex **1b** was evaluated *in vivo* by micronucleus (MN) testing on bone marrow cells and comet assay in peripheral blood lymphocytes and the results were compared with CDDP. The protective effect of extra virgin olive oil (EVOO) was also studied. The observations of genotoxicity clearly support the contention that copper-based drug candidate complex **1b** exhibits less cellular DNA damage as compared to the cisplatin drug. The present study demonstrate that studying the enantiomeric forms of biologically active copper complexes can provide a rationale for efficacious, less toxic and target-specific drug design therapy.

Acknowledgements

We express our gratitude to Department of Biotechnology, New Delhi, for generous financial support (scheme no. BT/PR9205/Med/30/13/2007). Our thanks are also due to (RSIC, Panjab University, Chandigarh) for NMR and ESIMS facility, RSIC, CDRI, Lucknow for providing the elemental analysis and IIT Mumbai for EPR measurements.

Notes and references

1 G. G. Hovhannisyan, T. S. Haroutunyan and R. M. Arutyunyan, *Exp. Oncol.*, 2004, **26**, 240–242.
2 C. X. Zhang and S. J. Lippard, *Curr. Opin. Chem. Biol.*, 2003, **7**, 481–489.
3 E. A. P. Gonzalez and A. G. Fuchs, *Dose-Response*, 2009, **7**, 234–246.
4 V. Srb, E. Kubzova and K. Kubikova, *Neoplasma*, 1986, **33**, 615–620.

5 C. Sanchez-Cano and M. J. Hannon, *Dalton Trans.*, 2009, 10702–10711.
6 C. G. Hartinger, S. Zorbas-Seifried, M. A. Jakupec, B. Kynast, H. Zorbas and B. K. Keppler, *J. Inorg. Biochem.*, 2006, **100**, 891–904.
7 E. Tomlinson, *Adv. Drug Delivery Rev.*, 1987, **1**, 87–198.
8 S. Thyagarajan, N. N. Murthy, A. A. N. Sarjeant, K. D. Karlin and S. E. Rokita, *J. Am. Chem. Soc.*, 2006, **128**, 7003–7008.
9 P. U. Maheswari, K. Lappalainen, M. Sfregola, S. Barends, P. Gamez, U. Turpeinen, I. Mutikainen, G. P. van Wezel and J. Reedijk, *Dalton Trans.*, 2007, 3676–3683; S. Dhar, P. A. N. Reddy, M. Nethaji, S. Mahadevan, M. K. Saha and A. R. Chakravarty, *Inorg. Chem.*, 2002, **41**, 3469–3476.
10 K. Nakamoto, *Infrared and Raman Spectra of Inorganic and Coordination Compounds*, Wiley-Interscience, New York, 1986.
11 G. Du, A. Ellern and L. K. Woo, *Inorg. Chem.*, 2003, **42**, 873–877.
12 U. Kumar, J. Thomas and N. Thirupathi, *Inorg. Chem.*, 2010, **49**, 62–72.
13 U. Mukhopadhyay and D. Ray, *Proc. – Indian Acad. Sci., Chem. Sci.*, 1998, **110**, 517–526.
14 R. Singh, A. Banerjee, E. Colacio and K. K. Rajak, *Inorg. Chem.*, 2009, **48**, 4753–4762.
15 S. Banerjee, S. Mondal, S. Sen, S. Das, D. L. Hughes, C. Rizzoli, C. Desplanches, C. Mandal and S. Mitra, *Dalton Trans.*, 2009, 6849–6860.
16 A. Ozarowski, I. B. Szymańska, T. Muzio and J. Jezierska, *J. Am. Chem. Soc.*, 2009, **131**, 10279–10292.
17 M. Trivedi, D. S. Pandey and N. P. Rath, *Inorg. Chim. Acta*, 2009, **362**, 284–290.
18 E. V. R. Akimova, A. Y. Nazarenko, L. Chen, P. W. Krieger, A. M. Herrera, V. V. Tarasov and P. D. Robinson, *Inorg. Chim. Acta*, 2001, **324**, 1–15.
19 A. W. Addison, T. N. Rao, J. Reedijk, J. van Rijn and G. C. Verschoor, *J. Chem. Soc., Dalton Trans.*, 1984, 1349–1356.
20 R. D. Willett, G. Pon and C. Nagy, *Inorg. Chem.*, 2001, **40**, 4342–4352.
21 Y. Zubavichus, M. Zharnikov, Y.-J. Yang, O. Fuchs, E. Umbach, C. Heske and M. Grunze, *Langmuir*, 2006, **22**, 7241–7247.
22 N. Grover, T. W. Welch, T. A. Fairley, M. Cory and H. H. Thorp, *Inorg.Chem.*, 1994, **33**, 3544–3548.
23 A. Raja, V. Rajendiran, P. U. Maheswari, R. Balamurugan, C. A. Kilner, M. A. Halcrow and M. Palaniandavar, *J. Inorg. Biochem.*, 2005, **99**, 1717–1732.
24 L.-F. Tan, H. Chao, K.-C. Zhen, J.-J. Fei, F. Wang, Y.-F. Zhou and L.-N. Ji, *Polyhedron*, 2007, **26**, 5458–5468.
25 G.-D. Liu, J.-P. Liao, Y.-Z. Fang, S.-S. Huang, G.-L. Sheng and R.-Q. Yu, *Anal. Sci.*, 2002, **18**, 391–395.
26 B. Norden and F. Tjerneld, *Biopolymers*, 1982, **21**, 1713–1734.
27 K. J. Humphreys, A. E. Johnson, K. D. Karlin and S. E. Rokita, *JBIC, J. Biol. Inorg. Chem.*, 2002, **7**, 835–842.
28 X. Dong, X. Wang, M. Lin, H. Sun, X. Yang and Z. Guo, *Inorg. Chem.*, 2010, **49**, 2541–2549.
29 T. Hirohama, Y. Kuranuki, E. Ebina, T. Sugizaki, H. Arii, M. Chikira, P. T. Selvi and M. Palaniandavar, *J. Inorg. Biochem.*, 2005, **99**, 1205–1219.
30 T. L. Overbeck, J. M. Knight and D. J. Beck, *Mutat. Res.*, 1996, **362**, 249–259.
31 L. M. Antunes, M. C. Araújo, J. D. Darin and M. L. Bianchi, *Mutat. Res.*, 2000, **465**, 131–137.
32 L. M. Antunes, L. M. Pascoal, M. De. L. Bianchi and F. L. Dias, *Mutat. Res.*, 2005, **585**, 113–119.
33 C. M. Evangelista, L. M. Antunes, H. D. Francescato and M. L. Bianchi, *Food Chem. Toxicol.*, 2004, **42**, 1291–1297.
34 R. W. Owen, A. Giacosa, W. E. Hull, R. Haubner, B. Spiegelhalder and H. Bartsch, *Eur. J. Cancer*, 2000, 1235–1247.
35 F. Visioli and C. Galli, *Crit. Rev. Food Sci. Nutr.*, 2002, **42**, 209–221.
36 K. Wozniak, A. Czechowska and J. Blasiak, *Chem.-Biol. Interact.*, 2004, **147**, 309–318.
37 A. M. J. Fichtinger-Schepman, A. T. van Oosterom, P. H. M. Lohman and F. Berends, *Cancer Res.*, 1987, **47**, 3000–3004.
38 M. Yoshida, A. Khokhar, Y. Kido, F. Ali-Osman and Z. Siddik, *Biochem. Pharmacol.*, 1994, **17**, 793–799.
39 Y. Sedletska, M.-J. Giraud-Panis and J.-M. Malinge, *Curr. Med. Chem.: Anti-Cancer Agents*, 2005, **5**, 251–265.
40 J. Marmur, *J. Mol. Biol.*, 1961, **3**, 208–214.
41 A. Wolfe, G. H. Shimer and T. Meehan, *Biochemistry*, 1987, **26**, 6392–6396.
42 J. R. Lakowiez and G. Webber, *Biochemistry*, 1973, **12**, 4161–4170.
43 F. Arjmand and M. Aziz, *Eur. J. Med. Chem.*, 2009, **44**, 834–844.
44 W. Schmid, *Mutat. Res.*, 1975, **31**, 9–15.
45 B. L. Pool-Zobel, C. Guigas, R. Klein, C. H. Neudecker, H. W. Renner and P. Schmezer, *Food Chem.Toxicol.*, 1993, **31**, 184–191.
46 N. P. Singh, M. T. McCoy, R. R. Tice and E. L. Schnieder, *Exp. Cell Res.*, 1998, **175**, 184–191.

